# Effect of the electrophoretic deposition of Au NPs in the performance CdS QDs sensitized solar Cells

I. Zarazua[1,3], D. Esparza[1], T. Lopez-Luke[1], eja-Fdez[1], J. Reyes-Gomez[2], I. Mora-Seró[3], and E. de la Rosa[1*]

[1]Centro de Investigaciones en Óptica, A.P. 1-948 León, Gto. 37150 MÉXICO,

[2]Facultad de Ciencias, Universidad de Colima, Colima, Col. 28045 MÉXICO,

[3]Institute of Advanced Materials, Universitat Jaume I, 12071 Castelló, Spain

**Corresponding author: elder@cio.mx**

## Abstract

Solution-processed mesoscopic oxide semiconductor-based materials offer potentially low-cost and high stability alternative for next generation of solar cells, and metallic nanoparticles had shown to be a good alternative to improve specific parameters in such kind of devices. In the present work, it is showed the systematic study of the effect of electrophoretic gold nanospheres (Au NPs) with cadmium sulfide Quantum Dots (CdS QDs) sensitized $TiO_2$ solar cells. Au NPs were added by electrophoretic deposition at several times (0.5, 2.5 and 7.5 minutes) and CdS QDs were deposited by a Successive Ionic Layer Absorption and Reaction (SILAR) method. Electrophoretic deposition allowed to significantly decrease the Au NPs deposition times respect previously reported methods. The results show that Au NPs reduce the photocurrent (from 9.85 to 9.44 mA/cm$^2$) at the same time that increase the open circuit voltage ($V_{oc}$) (from 575 to 618 mV) and the Fill Factor (FF) (from 46 to 51 %) which result in a final increase of the photoconversion efficiency (η) (from 2.63 to 2.96 % for 0.5 min of deposit). A systematic characterization permitted to identify the origin of the variations observed in the solar cell parameters with and without Au NPs. Incident Photon to Current conversion efficiency (IPCE) demonstrate that the Au NPs reduces the amount of light that reach the CdS QDs and Impedance Spectroscopy (IS) analysis, indicates a downshift in the $TiO_2$ conduction band (CB) and decreases the recombination processes, resulting in the observed increase in the FF and $V_{oc}$.

*Key words: Solar Cells, Quantum dots, Impedance spectroscopy, Au Nanoparticles*

## 1. Introduction

The semiconductor Quantum Dots (QDs) have attract significant attention as possible candidates for increase the energy conversion efficiency in the solar cells, since their theoretical maximum efficiency is 44% QDs, *e.g.*, CdSe, CdTe, CdS, PbS, PbSe, $Bi_2S_3$, and InP,[1-11] have been studied due to several advantage of the QDs, e.g.,have large extinction coefficients in the visible region and, after band gap excitation, undergo charge separation, injecting electrons to the conduction band of the metal oxide. QD-sensitized $TiO_2$ solar cells have been reported to have quantum efficiency (QE) as high as 80%, [1-11] reaching photoconversion efficiencies (η) of 8%.[3,12]. Thus, for such a configuration, it is necessary to improve the electron injection efficiency to increase η and take advantage of the QDs strong photoabsorption in the visible spectrum.

The photoresponse of semiconductors has also been improved with the presence of metallic NPs such as gold (Au) and silver (Ag), although the mechanism of the observed enhancement is not completely understood[3,5,13-20]. It has been suggested that such NPs enhance the visible-light-induced, electron-transfer process via Surface plasmon resonance.[3,21-28] However, mechanistic evidence that directly supports electron transfer arising from plasmon excitation remains elusive.[3,29,30] However, a strong increase in photoconversion efficiency with QD-sensitized Au-$TiO_2$ NP composite have been found which was attributed to enhanced absorption of QDs caused by increased scattering of light by the Au NPs[13,17]. Other authors, had found that Au NPs act as electron traps to help separate the photogenerated charges and subsequently improve interfacial charge transfer[10,16,31-33]. Studies also have shown a shift in the Fermi level to a more negative

level (in respect to vacuum) by doping the semiconductor with metal NPs. This shift enhances the efficiency of the interfacial charge transfer process [1,10,16,18,31-36]. In this case a 40% improvement of hole transfer efficiency from the semiconductor film to the electrolyte has been reported[2,4,6,8-10,31,37-41].

One of the motivations in PV cell studies is to understand the processes involved in the charge carrier transport inside the cell.[1,3,5,7] The semiconductor/electrolyte interface extends to the entire film volume, implying that transport, reaction, and polarization processes occurring throughout the porous structure of the film are coupled in an intricate manner.[3,12] Electrochemical impedance spectroscopy (EIS) is an excellent and well-established technique for characterizing electrochemical systems, most notably for those involving a number of coupled processes.[3,5,13-20] EIS can identify important parameters affecting the cell performance, such as: (i) electron transport in the $TiO_2$, which is influenced by the free carrier density and electron mobility, the latter being likely dependent on the carrier density, as the electron motion is a trap limited process,[3,21-23,25-28] (ii) transfer of electrons to redox species in the electrolyte (sometimes named *recombination* or *back reaction* process in the context of DSSC studies), (iii) charging of the contact on the transparent conducting substrate (TCS) with the electrolyte (provided that the electrolyte penetrates the porous structure up to the substrate), and (iv) charging of capacitive elements in the high surface area porous structure, including the Helmholtz capacitance in the $TiO_2$/electrolyte interface and the capacitances related to filling of the conduction band and surface states of the $TiO_2$ in the porous structure.[3,29,30] In addition, the lifetime, the diffusion coefficient, and the diffusion length could be obtained[13,17].

In this work, we report a systematic characterization of CdS QDs sensitized $TiO_2$ films

decorated with Au NPs at different times of electrophoretic deposition. The objective is to improve the overall photoconversion efficiency by extracting more efficiently the electrons from the QDs with the help of Au NPs. A detailed study of the structural, optical, and photoelectrochemical properties was carried out to gain new insight into the underlying mechanism. Impedance analyses indicate that Au NPs deposited by this method affect at the same time two parameters, reducing the recombination processes and downshifting position of the $TiO_2$'s CB, which result in an increase of the Voc, the electron transport and consequently the FF and η.

## 2. Experimental

### 2.1. Preparation of $TiO_2$ sensitized films

***Materials.***

$TiO_2$ Paste (WER2-0 Reflector) and $TiO_2$ Paste (DSL 18NR-T) were obtained from DYESOL, Titanium (IV) isopropoxide (97%), Acetylacetone (>99%), Cadmium acetate dehydrate ($Cd(CH_3COO)_2 \bullet 2H_2O$), Zinc acetate dihydrate ($Zn(CH_3COO)_2 \bullet 2H_2O$) and Sodium hydroxide (NaOH) were obtained from Sigma-Aldrich. Sulphur (S), and Sodium sulphide ($Na_2S \bullet 9H_2O$) were obtained from KARAL and Fluorine-doped tin oxide (FTO) TEC-15 by MTI.

***$TiO_2$ film Preparation.***

Fluorine-doped tin oxide (FTO) glasses were cleaned with water, acetone and ethanol in an ultrasonic bath for 15 min each before use. All the photoelectrodes were made of three different $TiO_2$ layers stacked one on the top of the other. 1) Compact layer: A solution of

titanium (IV) Isopropoxide (0.2M) in acetylacetone/ethanol (1:1 V:V) deposited by spray pyrolysis over an FTO and sintered at 450 °C for 30 min to obtain a 190 nm layer. This layer will avoid shortcuts reducing the recombination processes between the electrolyte and the FTO. 2) Transparent layer: $TiO_2$ paste, (DSL 18-NRT, 20 nm average particle size) is deposited over the compact layer by Doctor Blade method obtaining a 6µm thick film. This layer will be the active layer i. e. where the sensitizers will be adsorbed and the mayor of the photo absorption process will be done. And 3) Scattering layer: a 9 µm layer is obtained by doctor blading depositing Wer2-O Reflector paste (400 nm particle size). This last layer will scatter the light that has passed through the first two layers without been absorbed, giving a second chance to be absorbed by the QDs. [4,11,42,43] The films were sintered for 30 min at 450 °C to obtain a good electrical contact between nanoparticles.

***Au nanoparticles synthesis***.

The synthesis of Au NPs was based on the Turkevich method, by adding 3.75 ml of 1%wt. sodium citrate solution to a 0.001M $HAuCl_4$ boiling solution and stirring at 500 rpm, until ruby red solution. Then the solution was cooled to room temperature and filtered. With this procedure13 nm particles were obtained. The size and shape were verified via UV-Vis absorption spectroscopy and TEM.

***Au deposit***

After synthesis, the Au NPs were deposited on the $TiO_2$ films by electrophoresis. The samples were placed face to face with an FTO at distance of 0.2 cm and inserted in a cuvette with 2.5 mL of a colloidal suspension of the corresponding Au nanoparticles. Next, a 5V DC voltage was applied between the $TiO_2$ films for several deposition times.

***Film sensitization:***

The $TiO_2$/Au Nps electrodes were in situ sensitized with CdS QDs grown by SILAR. For this purpose, solutions of 0.05M $Cd(CH_3COO)_2$ dissolved in ethanol as $Cd^{2+}$ source and 0.05 M $Na_2S$ in methanol:water (V:V = 1:1) as $S^{2-}$ source, were used. A single SILAR cycle consisted of 1 min dip-coating the $TiO_2$ electrode into the cadmium solution ($Cd^{2+}$) and subsequently into the sulfide solutions, also during 1 min. After each dipping step in a precursor solution, the electrodes were thoroughly rinsed by immersion in the corresponding solvent in order to remove the excess of precursor. Seven SILAR cycles were done to obtain a uniform coverage of the $TiO_2$ NPs with CdS QDs. To enhance the photovoltaic performance ZnS is deposited by SILAR for passivate CdS surface and reduce the recombination of electrons in the $TiO_2$ to the polysulfide electrolyte [1,10,16,18,31-33,35,36]. ZnS passivation was obtained by using 0.1M of $Zn(CH_3COO)_2 \bullet 2H_2O$ and 0.1 M of $Na_2S$ both dissolved in water as $Zn^{2+}$ and $S^{2-}$ sources respectively. The films were dipped for 1 min/dip in the solutions during 2 SILAR cycles.

***Counter electrode manufacturing and assembling of solar cells***:

$Cu_2S$ counter electrodes were fabricated by immersing brass foil in an HCl solution (38% by volume) at 90 ºC for 1 hour. These substrates were sulfated by adding a drop of poly-sulfide electrolyte solution made by mixing solutions of $Na_2S$ (1 M), S (1.0 M), and NaOH (0.1 M) in distilled water. The solar cells were constructed by assembling the $Cu_2S$ counter electrode and the sensitized $TiO_2$ film electrode with a binder clip separated by a scotch spacer. Lastly, a polysulfide electrolyte was introduced by dropping into the solar cell.

### 2.2. Characterization

Transmission Electron Microscopy (TEM) images were obtained from a FEI- Titan 80-300 KeV, microscope, equipped with ultra-stable Schottky field emitter gun. The UV-vis absorption spectra of the colloidal Au NPs were measured by transmittance and substrates were measured by diffuse reflectance in the range of 360 nm to 800 nm using an Agilent Technologies Cary Series UV-Vis-NIR spectrophotometer (Cary 5000) and an integrating sphere of 60 mm. The current density curves were measured with a reference 600 Gamry potensiotat, scanning from 0 to 600 mV at 100 mV/S. The samples were illuminated with an Oriel Sol 3A solar simulator while measuring. The light intensity was adjusted employing a NREL calibrated Si solar cell having KG-2 filter for one sun light intensity (100 mW/cm$^2$). Best results are reported. IPCE spectra measurements were made with a monochromator (Newport model 74125). Electrochemical Impendance Spectroscopy (EIS) measurements were carried out by applying a small voltage perturbation (10 mV) at frequencies from 100 Hz to 0.1 Hz for different forward bias voltages in dark conditions.

## 3. Results

### 3.1. Structural and Morphological Characterization

**Au Nanostructured particles**

The representative electron microscopy images from the gold nanostructured particles are shown in Figure 1. Nanospheres (NPs) have typically 12 nm of diameter and have good size confinement

**$TiO_2$ films**

In Figure 2 are presented SEM images of the transparent layer of the $TiO_2$ films. It can be seen that when not decorated (Figure 2 a) the films are composed for 35nm average size $TiO_2$ NPs agglomerated in a homogenous high porous arrangement. When Au NPs are electrophoretic deposited (see Figure 2 b), spherical particles of approximately 13 nm are observed on the film indifferently of the polarity applied to the sample during the deposit. The size and shape of the nanoparticles indicate that they are Au NPs. When the films are SILAR sensitized the $TiO_2$ NPs are completely covered by the CdS QDs, partially filling the spaces between the particles. This gives the films a soft and less porous appearance (see Figure 2 c). Finally, when the films are decorated with Au NPs and sensitized with CdS to form $TiO_2$/Au/CdS samples (Figure 2 d), a uniform coverage of the film with the QDs is obtained. But the appearance of the deposit is gnarled due to the presence of the Au NPs. EDS analyses of the films (Figure 2 e) confirm the presence of the Au NPs and Cd and S from the QDs.

**Optical Absorption**

The absorption spectra of the Au NPs, bare $TiO_2$ films, CdS QDs sensitized $TiO_2$ films, 2.5 minutes Au NPs electrophoretic decorated films, Au decorated/ CdS QDs sensitized $TiO_2$ films are shown in Figure 3. The Au NPs abortion (red circles) presents a well-defined peak at 519 nm that is consistent with the surface plasmon resonance (SPR) for such size of NPs. The $TiO_2$ films (black solid line) have almost no absorption in the visible region, rapidly increasing for wavelengths ($\lambda$) lower than 400 nm. When Au NPs deposit is done for 2.5 min (orange +) there is a uniform increase in the absorption between 380 and 800 nm,

pointing to a light scattering effect. While, CdS sensitization of the $TiO_2$ films (blue doted line) produces an absorption shoulder from 400 to 500 nm, which corresponds to the absorption of the CdS QDs[1,12,24,34]. Finally, when CdS sensitization is done in 2.5 min Au NPs decorated films, the shape in obtained spectra is similar to the films only sensitized with CdS QDs. But have a general increase in the absorption in the visible region, this increase match with the increase obtained in samples only decorated with Au NPs (orange +).

### 3.2. Photoelectrical Conversion Measurements

**J-V Curves**

Figure 4 shows the current density-voltage (J-V) profiles of the $TiO_2$ films decorated by electrophoresis with Au NPs and further sensitized with CdS QDs ($TiO_2$/Au/CdS) at several deposition times. Fill Factor (FF) and photoelectrical conversion efficiency (η) were calculated using Eq. 1 and Eq. 2 for short-circuit current density ($J_{sc}$) and open-circuit voltage ($V_{oc}$) obtained from the curves[12-16,18,44,45]

$$FF = \frac{P_m}{J_{sc} x V_{oc}} x100 \quad (1)$$

$$\eta = \frac{P_m}{P_i} x100 = FF \frac{J_{sc} x V_{oc}}{P_i} \quad (2)$$

where, $P_m$ is the maximum power (J×V product) observed from the current density-voltage curve for each device and $P_i$ is the incident light power density (100 mW×cm$^{-2}$). Four

samples of each configuration were measured, finding a maximum relative standard deviation of 1.8%. Champion values are listed in Table 1.

Analyzing the curves, it can be seen than the $TiO_2$/CdS films (black line), have a $J_{sc}$ of 9.85 mA/cm$^2$ an $V_{oc}$ of 575 mV, a FF of 46.5% and a photoconversion efficiency of 2.63%, which is in good agreement with the efficiencies reported for this kind of solar cells[13,14,16,18,46-49]. When a 30s Au NPs deposit is applied ($TiO_2$/Au(0.5)/CdS), a small reduction in the photocurrent is obtained ($J_{sc}$ 9.5 mA) maintaining relatively constant for longer deposition times (9.5 and 9.4 mA for 2.5 and 7.5 min respectively). At the same time, the Au NPs deposit increases the $V_{oc}$ to 612 mV at 30 seconds of deposit. Maintaining almost constant for 2.5 min of deposit (618 mV) and reducing for higher times (570 mV for 7.5 min). In a similar way, the Au NPs deposit increases the FF to 51.0% with the first 30 seconds of electrophoresis, and maintaining almost constant for higher deposition times (50 and 50.3 for 2.5 and 7.5 min respectively). Finally, to test the deposition order effect, $TiO_2$/CdS/Au samples were made. Inset in Figure 4 shows the champion cells of each configuration ($TiO_2$/CdS ,$TiO_2$/CdS/Au and $TiO_2$ /Au/CdS). It can be seen that Au NPs addition after CdS sensitization result in a general reduction of the cell performance, possibly due to a partial removing or damage of the QDs.

**IPCE Characterization**

$J_{sc}$ is mainly dominated by two phenomena, the photogeneration (i.e. the process where photons are absorbed to generate electron hole pairs) and the injection (the transference of the electrons and holes from the photogenerator to the electron and hole transporter respectively). To understand the photogeneration in terms of the contribution of each

wavelength, the incident photon to current conversion efficiency (IPCE), A.K.A.external quantum efficiency (QE), was calculated by was calculated by the expression.

$$IPCE(\%) = \frac{1240\ x\ J_{sc}(mA/cm^2)}{\lambda(nm) x\ P_{inc}(mW/cm^2)}\ x\ 100 \qquad (3),$$

Where $P_{inc}$ stand for the light incident power. Figure 5 shows the IPCE curves TiO2/Au/CdS samples. Here it can be appreciated that samples without Au NPs have a QE higher than 60% in the 380-530nm, reaching it maximum at 460 nm (QE=72%) and rapidly decreasing for λ>550 nm.With 0.5 min of Au NPs deposit (green line) a reduction in the QE in the 380-530 nm region is obtained with an small increase over a wide range of wavelengths between 550 and 700 nm, when the deposition time is increased to 2.5 min (blue line) it is obtained almost the same spectrum than for 0.5 min but without the contribution in the 550 to 700 nm. With higher deposition times (7.5 min, pink line) a stronger reduction of QE are observed. These reductions in the QE are consistent with the reductions in Jsc. These results in conjunction with the absorbance curves indicate that a small coverage with Au NPs could increase the photoabsorption of the CdS or electron injection into the mesoscopic $TiO_2$ due to the good conductivity of Au NPs. While for higher coverage Au NPs act as an optical filter reducing the amount of light reaching the absorbing elements ($TiO_2$ and QDs).

**Electrochemical Impedance**

Electrochemical impedance spectroscopy (EIS) measurements were carried out to explain the trends observed in the solar cell parameters (particularly $V_{oc}$ and FF) in terms of

the internal physical processes when Au Nanoparticles are deposited. To do appropriate fit the EIS measurements, the equivalent circuit shown in Figure 6 was used [5,21,23,24,26,50-52] Where $R_s$ is the series resistance and is related to the resistance of FTO and the wires resistance, $R_{con}$ and $C_{con}$ are the resistance and capacitance associated to the charge transfer in the counter electrode, $R_t$ ($=r_t/L$) is the transport resistance, and is related with the resistance to the electron flux inside of $TiO_2$/sensitizer composite, which include the electron transport inside of the nanostructured particles, and between the nanostructured particles. $R_{rec}$ ($=r_{rec}/L$) and $C_\mu$ ($=c_\mu L$) are the charge transfer resistance and the chemical capacitance respectively. Where $R_{rec}$ is inversely proportional to the recombination rate. These last three mentioned elements are denoted in lowercase letters in figure 6 meaning the element per unit length for a film of thickness L, because they are distributed in a repetitive arrangement of a transmission line.

$C_\mu$, $R_{rec}$ and $R_t$ extracted from the EIS fitting of the CdS and Au/CdS sensitized solar cells are shown in Figure 7. Cμ is represented versus the applied voltage ($V_{app}$) less the voltage drop due to FTO and wire resistance at the photoanode ($V_{series}=R_s x J$). Then the new voltage is defined as $V_f=V_{app}-V_{series}$ [29,50,53,54]. The chemical capacitance is proportional to the density of states (DOS) in the band gap, DOS increases exponentially with the proximity to the conduction band (CB), then, an increase in $C_\mu$ suggest a displacement to lower energies of the $TiO_2$ CB. $R_{rec}$ and $R_t$ are exponentially dependent on carrier density (i.e. the distance to CB), then, to correctly evaluate this parameters a new potential is defined where, the measurements are at the same equivalent value of position to the CB of each device, using the equation [13,54].

$$V_{ecb} = V_F - \Delta V_i \quad (4),$$

Where ecb means equivalent conduction band and $\Delta V_i$ is the voltage shift observed between the Au decorated samples and the CdS sensitized film in Figure 7 a. After the voltage correction Cμ overlaps as shown in the inset of Figure 7 omparing $R_{rec}$ and $C_\mu$ for the cells, it is viable to understand the origin in the $V_{oc}$ variation. [10,16,31-33,50]. Higher $V_{oc}$ observed in Au decorated cells could be due to three processes: (1) An increase in the absorption. (2) A shift in the $TiO_2$ CB, and/ or (3) a change in the recombination rate. An increase in the photo absorption will result in an increase in $J_{sc}$ and $V_{oc}$. As previously discussed the photoabsorption in these samples is reduced. Then, hypothesis 1 can be discarded

The second effect, a shift in the $TiO_2$ CB, produces a movement of the $TiO_2$ electron quasi-Fermi level, which determines the $V_{oc}$, then an upward of the $TiO_2$ CB will mean an increase in the $V_{oc}$. This upward displacement of the conduction band is identified, by a shift to higher potentials of $C_\mu$ (i.e. a reduction of the capacitance). When Au are deposited, a general increase in Cμ is observed (see Figure 7 a) which means a downshift in the conduction band and the $V_{oc}$. It is observed that for short depositions times (0.5 min) a downshift of about 85 mV is obtained (green circles), when the deposition time is increased to 2.5 min the band shift increases to approximately 175 mV (blue triangles). Finally, for higher deposition times, a reduction in the shift is obtained (135 mV at 7.5 min). These results as the obtained for $J_{sc}$ contravene the observed $V_{oc}$ behavior of such samples, indicating that the photocurrent is not the dominant process in the $V_{oc}$ variations.

The third effect, the recombination rate, can be also determined with EIS by analyzing the $R_{rec}$. Where an increase in this parameter indicates a reduction in the electron recombination processes from the $TiO_2$ CB to acceptor states either in the electrolyte or the sensitizer[34,54]. Comparing $TiO_2$/Au/CdS and $TiO_2$/CdS samples in Figure 7b, it is

observed that with 0.5 min of deposit $R_{rec}$ increases (green circles), indicating an increase of the $V_{oc}$. When the deposition time is increased to 2.5 min a higher increase in $R_{rec}$ is obtained (blue triangles). If the deposition time still increasing (7.5 min) $R_{rec}$ have a small reduction, resulting in a resistance a little lower than the obtained for the samples with 0.5 min of deposit. Analyzing these same results in the $V_{ecb}$ convention, it is observed that with the first 30 seconds of Au NPs deposit the increase in $R_{rec}$ is stronger than the observed in the $V_f$ convention, and when the deposition time is increased to 2.5 min still increasing, while for 7.5 min of Au NPs deposit $R_{rec}$ drops until reach the resistance obtained for 0.5 min of deposit. These results imply that the observed increases in $R_{rec}$ in the $V_f$ convention are the result of strong reductions in the recombination processes (possibly due to a passivation of the $TiO_2$ superficial defects) that are slightly masked by the $TiO_2$'s CB displacement.

Then, when Au NPs are deposited, two simultaneous processes affect the $V_{oc}$. On one side the $TiO_2$ CB is downshifted reducing the $V_{oc}$, but at the same time Recombination processes are considerably reduced upshifting the Fermi level and the $V_{oc}$. At the end the reduction of recombination processes overcome the effect of the CB shift increasing the photovoltage.

Another important parameter that is positively affected by the Au deposit is the FF. Variations in this parameter can be due to changes in the Transport resistance ($R_t$), where a reduction in $R_t$ results in a FF increment [2,4,6,8-10,31,37-41,50]. The $R_t$ behavior in the samples (Figure 7 c) indicate that for 30 seconds of Au NPs deposit (green circles) slightly reduces $R_t$, with the increase in the deposition time $R_t$ increases until the 7.5 minutes deposit, when $R_t$ reaches the same level than samples without Au NPs deposit indicating an increase in the electron transport (and the FF) with the first 30s of Au NPs deposit and an

slow reduction of these parameter with higher deposition times, which match with the behavior observed in table 1. Analyzing these curves in the $V_{ecb}$ convention (inset of Figure 7 c) it could be appreciated than the Au deposit increases the resistance to the electron flux, this suggest that Au NPs pore filling is hindering the movement of the electrolyte ions affecting the electron motion in the $TiO_2$. However, the CB shift produces an effective increase in the electron flux that overcompensates the Au NPs pore filling effect resulting in the increase of the FF.

## 4. Discussion

In summary, when a photon of visible light (λ = 370-570 nm) insides on the CdS QDs of $TiO_2$/CdS samples, an electron hole pair is generated (see Figure 8 a), the electron is injected from the CdS QD's CB to the $TiO_2$'s CB driven by the energy difference between the bands Δχ, then it will be transported by the $TiO_2$ and in an ideal case to the FTO and the electrical circuit. However, some electrons interact whit trap levels in the QD/$TiO_2$, giving a recombination process (red arrow in Figure 8 a ) reducing the performance of the cell. In the other side, holes are taken by the electrolyte via the oxidation of the $S_{x-1}^{2-}$ ions, as shown in the Figure 8a. After that, the resulting $S_x^{2-}$ ions moved by diffusion to the counter electrode where they are reduced to $S_{x-1}^{2-}$ ions and the circuit is closed. As previously discussed, in these conditions $J_{sc}$ is principally determined by the photogeneration process (the amount of photons that inside in the QDs and the efficiency to convert such photons in electron hole pairs), and the injection process (driven by Δχ). Meanwhile, the $V_{oc}$ is due to the energy difference between the Fermi level of the $TiO_2$ ($E_F$) and the redox level. Finally, the FF will be determined by the ratio of the transport and recombination processes.

When Au NPs are deposited various simultaneous processes occurred (Figure 8 b). (1) Au NPs act as an optical filter, reducing the amount of light that reaches the CdS QDs, which will result in a reduction of $J_{sc}$. (2) The $TiO_2$ CB is downshifted by the energy levels equilibration process. This band movement will affect at the same time three parameters, $J_{sc}$ is slightly increased by the increase in the potential energy between the sensitizer and the $TiO_2$ ($\Delta\chi$), $V_{oc}$ is reduced by the downshift of $E_F$, and the FF is considerable increased by a reduction in the transport resistance. (3) The recombination processes are considerably reduced, resulting in higher amount of electrons in the $TiO_2$'s CB; this upshifts $E_F$ and increments $V_{oc}$. Then, when these three processes are combined in the right proportion what is obtained is a reduction in $J_{sc}$, an increase in $V_{oc}$ and an increase in FF that together give an increase in the photoconversion efficiency from 2.6 to 2.9%.

## 5. Conclusions

The photovoltaic properties of CdS QD-sensitized $TiO_2$ NC films decorated by electrophoresis with Au NPs at different deposition times have been systematically studied and analyzed. It was demonstrated that Au NPs could improve the photoconversion efficiency of $TiO_2$/CdS QDs films when applied very short deposition times (30 seconds), by increasing $V_{oc}$ and FF sacrificing $J_{sc}$. IPCE measurements show that the presence of Au NPs reduces the capacity of the CdS QDs to absorb light, and impedance spectroscopy analyses indicates that Au NPs at the same time moves down the $TiO_2$'s CB and reduces the recombination processes. The band movement helps to reduce the photocurrent losses

due to the absorption issue, and the reduction in the recombination processes give the observed increase in $V_{oc}$ (from 575 to 611 mV) and FF (from 46 to 50 %), that result in the final increase in η from 2.6 to 2.9 % .

## Acknowledgments:

We acknowledge financial support from CONACYT through grant 134111, the UC-MEXUS program grant 00007, the European Community Seven Framework Program (FP7-428 NMP-2010-EU-MEXICO), CIO-UGTO 2013 y 2014 and the CEMIE-Solar (04002) consortium. D. Esparza, and eja acknowledge scholarship from CONACYT and thanks to Maria Christian Albor for SEM and EDS analysis. Isaac Zarazúa thanks to CONACYT for the postdoctoral fellow.

## References


[1] V. González-Pedro, C. Sima, G. Marzari, P.P. Boix, S. Giménez, Q. Shen, et al., High performance PbS Quantum Dot Sensitized Solar Cells exceeding 4% efficiency: the role of metal precursors in the electron injection and charge separation, Phys. Chem. Chem. Phys. 15 (2013) 13835. doi:10.1039/c3cp51651b.

[2] A. Kongkanand, K. Tvrdy, K. Takechi, M. Kuno, P.V. Kamat, Quantum Dot Solar Cells. Tuning Photoresponse through Size and Shape Control of CdSe-$TiO_2$ Architecture, J. Am. Chem. Soc. 130 (2008) 4007–4015.

[3] F. Fabregat-Santiago, G. Garcia-Belmonte, J. Bisquert, A. Zaban, P. Salvador, Decoupling of Transport, Charge Storage, and Interfacial Charge Transfer in the Nanocrystalline TiO 2/Electrolyte System by Impedance Methods, J. Phys. Chem. B. 106 (2002) 334–339. doi:10.1021/jp0119429.

[4] I. Mora-Seró, T. Dittrich, A. Susha, A. Rogach, J. Bisquert, Large improvement of electron extraction from CdSe quantum dots into a $TiO_2$ thin layer by N3 dye coabsorption, Thin Solid Films. 516 (2008) 6994–6998.

[5] F. Fabregat-Santiago, J. Bisquert, G. Garcia-Belmonte, G. Boschloo, A. Hagfeldt, Influence of electrolyte in transport and recombination in dye-sensitized solar cells studied by impedance spectroscopy, Sol. Energy Mater. Sol. Cells. 87 (2005) 117–131. doi:10.1016/j.solmat.2004.07.017.

[6] T. Lopez-Luke, A. Wolcott, L. Xu, S. Chen, Z. Wen, J. Li, et al., Nitrogen-doped and CdSe quantum-dot-sensitized nanocrystalline $TiO_2$ films for solar energy conversion applications, J. Phys. Chem. C. 112 (2008) 1282–1292.

[7] P.P. Boix, G. Larramona, A. Jacob, B. Delatouche, I. Mora-Sero, J. Bisquert, Hole Transport and Recombination in All-Solid Sb 2S 3-Sensitized TiO 2Solar Cells Using CuSCN As Hole Transporter, J. Phys. Chem. C. 116 (2012) 1579–1587. doi:10.1021/jp210002c.

[8] T. Zeng, S. Liu, F. Hsu, K. Huang, H. Liao, Effects of bifunctional linker on the performance of P3HT/CdSe quantum dot-linker-ZnO nanocolumn photovoltaic

device, Opt. Express. 18 (2010) 130137.

[9] A. Franceschetti, J. An, A. Zunger, Impact ionization can explain carrier multiplication in PbSe quantum dots, Nano. Lett. 6 (2006) 2191–2195.

[10] I. Zarazúa, E. De La Rosa, T. Lopez-Luke, J. Reyes-Gomez, S. Ruiz, C. Angeles Chavez, et al., Photovoltaic Conversion Enhancement of CdSe Quantum Dot-Sensitized $TiO_2$ Decorated with Au Nanoparticles and P3OT, J. Phys. Chem. C. 115 (2011) 23209–23220.

[11] D. Esparza, I. Zarazúa, T. Lopez-Luke, R. Carriles, Photovoltaic Properties of Bi2S3 and CdS Quantum Dot Sensitized TiO2 Solar Cells, Electrochimical Acta. (2015) 486–492.

[12] C. Chuang, P.R. Brown, V. Bulović, M.G. Bawendi, Improved performance and stability in quantum dot solar cells through band alignment engineering : Nature Materials : Nature Publishing Group, Nature Mater. (2014).

[13] L. Liu, G. Wang, Y. Li, Y. Li, J.Z. Zhang, CdSe quantum dot-sensitized Au/$TiO_2$ hybrid mesoporous films and their enhanced photoelectrochemical performance, Nano Research. (2011) 1–10.

[14] G. Zhao, H. Kozuka, T. Yoko, Photoelectrochemical properties of dye-sensitized TiO2 films containing dispersed gold metal particles prepared by sol-gel method, Nippon Seramikkusu Kyokai Gakujutsu Ronbunshi. 104 (1996) 164–168.

[15] Y. Nakato, M. Shioji, H. Tsubomura, Photoeffects on the potentials of thin metal films on a n-TiO2 crystal wafer. The mechanism of semiconductor photocatalysts, Chem. Phys. Lett. 90 (1982) 453–456. doi:10.1016/0009-2614(82)80253-4.

[16] N. Chandrasekharan, P.V. Kamat, Improving the Photoelectrochemical Performance of Nanostructured $TiO_2$ Films by Adsorption of Gold Nanoparticles†, J. Phys. Chem. B. 104 (2000) 10851.

[17] C. He, Z. Zheng, H. Tang, L. Zhao, Electrochemical impedance spectroscopy characterization of electron transport and recombination in ZnO nanorod dye-sensitized solar cells, J. Phys. Chem. C. 113 (2009) 10322–10325.

[18] Y. Tian, T. Tatsuma, Mechanisms and Applications of Plasmon-Induced Charge Separation at $TiO_2$ Films Loaded with Gold Nanoparticles, J. Am. Chem. Soc. 127 (2005) 7632–7637. doi:10.1021/ja042192u.

[19] Y.Y. Proskuryakov, K. Durose, M.K. Al Turkestani, I. Mora-Seró, G. Garcia-Belmonte, F. Fabregat-Santiago, et al., Impedance spectroscopy of thin-film CdTe/CdS solar cells under varied illumination, J. Appl. Phys. 106 (2009) 044507. doi:10.1063/1.3204484.

[20] I. Mora-Sero, Y. Luo, G. Garcia-Belmonte, J. Bisquert, D. Muñoz, C. Voz, et al., Recombination rates in heterojunction silicon solar cells analyzed by impedance spectroscopy at forward bias and under illumination, Sol. Energy Mater. Sol. Cells. 92 (2008) 505–509. doi:10.1016/j.solmat.2007.11.005.

[21] A. Liu, Q. Ren, M. Zhao, T. Xu, M. Yuan, T. Zhao, Photovoltaic performance enhancement of CdS quantum dot-sensitized TiO2 photoanodes with plasmonic gold nanoparticles, Journal of Alloys and …. (2014).

[22] P. de Jongh, D. Vanmaekelbergh, Trap-Limited Electronic Transport in Assemblies of Nanometer-Size TiO2 Particles, Phys. Rev. Lett. 77 (1996) 3427–3430. doi:10.1103/PhysRevLett.77.3427.

[23] W.-L. Liu, F.-C. Lin, Y.-C. Yang, C.-H. Huang, S. Gwo, M.H. Huang, et al., Influence of morphology on the plasmonic enhancement effect of Au@TiO2 core-shell nanoparticles in dye-sensitized solar cells, arXiv. cond-mat.mtrl-sci (2013).

[24] P.N. Kumar, R. Narayanan, M. Deepa, A.K. Srivastava, Au@poly(acrylic acid) plasmons and C60 improve the light harvesting capability of a TiO2/CdS/CdSeS photoanode, J. Mater. Chem. A. 2 (2014) 9771. doi:10.1039/c4ta01140f.

[25] R. Könenkamp, R. Henninger, Recombination in nanophase TiO2 films, Applied Physics A. 58 (1994) 87–90.

[26] Y. Nishijima, K. Ueno, Y. Yokota, Plasmon-Assisted Photocurrent Generation from Visible to Near-Infrared Wavelength Using a Au-Nanorods/$TiO_2$ Electrode, J. Phys. Chem. Lett. (2010).

[27] R. Könenkamp, Carrier transport in nanoporous TiO2 films, Phys. Rev. B. 61 (2000) 11057–11064. doi:10.1103/PhysRevB.61.11057.

[28] J. van de Lagemaat, A.J. Frank, Effect of the Surface-State Distribution on Electron Transport in Dye-Sensitized TiO 2Solar Cells: Nonlinear Electron-Transport Kinetics, J. Phys. Chem. B. 104 (2000) 4292–4294. doi:10.1021/jp000836o.

[29] Y.-S. Chen, H. Choi, P.V. Kamat, Metal-Cluster-Sensitized Solar Cells. A New Class of Thiolated Gold Sensitizers Delivering Efficiency Greater Than 2%, J. Am. Chem. Soc. 135 (2013) 8822–8825. doi:10.1021/ja403807f.

[30] G. Franco, J. Gehring, L.M. Peter, E.A. Ponomarev, I. Uhlendorf, Frequency-Resolved Optical Detection of Photoinjected Electrons in Dye-Sensitized Nanocrystalline Photovoltaic Cells, J. Phys. Chem. B. 103 (1999) 692–698. doi:10.1021/jp984060r.

[31] A. Dawson, P.V. Kamat, Semiconductor− Metal Nanocomposites. Photoinduced Fusion and Photocatalysis of Gold-Capped $TiO_2$ ($TiO_2$/Gold) Nanoparticles, J. Phys. Chem. B. (2001).

[32] V. Subramanian, E. Wolf, P.V. Kamat, Semiconductor-Metal Composite Nanostructures. To What Extent Do Metal Nanoparticles Improve the Photocatalytic Activity of $TiO_2$ Films? J. Phys. Chem. B. 105 (2001) 11439–11446.

[33] I. Zarazúa, T. Lopez-Luke, J. Reyes-Gomez, A. Torres Castro, J.Z. Zhang, E. De la Rosa, Impedance Analysis of CdSe Quantum Dot-Sensitized TiO2 Solar Cells Decorated with Au Nanoparticles and P3OT, Journal of the Electrochemical Society. (2014).

[34] G. Burgeth, H. Kisch, Photocatalytic and photoelectrochemical properties of titania–chloroplatinate(IV), Coordination Chemistry Reviews. 230 (2002) 41–47. doi:10.1016/S0010-8545(02)00095-4.

[35] I. Mora-Sero, S. Giménez, F. Fabregat-Santiago, R. Gomez, Q. Shen, T. Toyoda, et al., Recombination in Quantum Dot Sensitized Solar Cells, Acc. Chem. Res. 42 (2009) 1848–1857. doi:10.1021/ar900134d.

[36] N. Guijarro, J.M. Campiña, Q. Shen, T. Toyoda, T. Lana-Villarreal, R. Gomez, Uncovering the role of the ZnS treatment in the performance of quantum dot sensitized solar cells, Phys. Chem. Chem. Phys. 13 (2011) 12024. doi:10.1039/c1cp20290a.

[37] I. Robel, V. Subramanian, M. Kuno, P.V. Kamat, Quantum dot solar cells. Harvesting light energy with CdSe nanocrystals molecularly linked to mesoscopic $TiO_2$ films, J. Am. Chem. Soc. 128 (2006) 2385–2393.

[38] P.V. Kamat, Quantum Dot Solar Cells. Semiconductor Nanocrystals as Light

Harvesters, J. Phys. Chem. C. 112 (2008) 18737–18753.

[39] M. Sykora, M.A. Petruska, J. Alstrum-Acevedo, I. Bezel, T.J. Meyer, V.I. Klimov, Photoinduced Charge Transfer between CdSe Nanocrystal Quantum Dots and Ru-Polypyridine Complexes, J. Am. Chem. Soc. 128 (2006) 9984–9985.

[40] R. Loef, A.J. Houtepen, E. Talgorn, J. Schoonman, A. Goossens, Study of Electronic Defects in CdSe Quantum Dots and Their Involvement in Quantum Dot Solar Cells, Nano. Lett. 9 (2009) 956–859.

[41] N. Guijarro, T. Lana-Villarreal, I. Mora-Sero, J. Bisquert, R. Gomez, CdSe Quantum Dot-Sensitized $TiO_2$ Electrodes: Effect of Quantum Dot Coverage and Mode of Attachment, J. Phys. Chem. C. 113 (2009) 4208–4214.

[42] A. Cerdán-Pasarán, T. Lopez-luke, D. Esparza, I. Zarazúa, E. De la Rosa, R. Fuentes-Ramírez, et al., Photovoltaic properties of multilayered quantum dot/quantum rod-sensitized TiO 2solar cells fabricated by SILAR and electrophoresis, Phys. Chem. Chem. Phys. 17 (2015) 18590–18599. doi:10.1039/C5CP02541A.

[43] D. Esparza, I. Zarazúa, T. Lopez-luke, A. Cerdán-Pasarán, A. Sánchez-Solís, A. Torres-Castro, et al., Effect of Different Sensitization Technique on the Photoconversion Efficiency of CdS Quantum Dot and CdSe Quantum Rod Sensitized TiO 2Solar Cells, J. Phys. Chem. C. 119 (2015) 13394–13403. doi:10.1021/acs.jpcc.5b01525.

[44] T. Soga, Nanostructured Materials for Solar Energy Conversion, Elsevier, Burlington, MA, 2007.

[45] J. Nelson, The physics of solar cells, Imperial college press, 2003.

[46] N. Parsi Benehkohal, V. González-Pedro, P.P. Boix, S. Chavhan, R. Tena-Zaera, G.P. Demopoulos, et al., Colloidal PbS and PbSeS Quantum Dot Sensitized Solar Cells Prepared by Electrophoretic Deposition, J. Phys. Chem. C. 116 (2012) 16391–16397. doi:10.1021/jp3056009.

[47] Mahmoud Samadpour, P.P. Boix, S. Gimenez, Azam Iraji Zad, Nima Taghavinia, Ivan Mora-Sero, et al., Fluorine Treatment of TiO2 for Enhancing Quantum Dot Sensitized Solar Cell Performance, J. Phys. Chem. C. 115 (2011) 14400–14407. doi:10.1021/jp202819y.

[48] A. Braga, S. Giménez, I. Concina, A. Vomiero, I. Mora-Sero, Panchromatic Sensitized Solar Cells Based on Metal Sulfide Quantum Dots Grown Directly on Nanostructured $TiO_2$ Electrodes, J. Phys. Chem. Lett. 2 (2011) 454–460. doi:10.1021/jz2000112.

[49] M. Solis de la Fuente, R.S. Sanchez, V. González-Pedro, P.P. Boix, S.G. Mhaisalkar, M.E. Rincón, et al., Effect of Organic and Inorganic Passivation in Quantum-Dot-Sensitized Solar Cells, J. Phys. Chem. Lett. 4 (2013) 1519–1525. doi:10.1021/jz400626r.

[50] S. Giménez, T. Lana-Villarreal, R. Gomez, S. Agouram, V. Muñoz-Sanjosé, I. Mora-Sero, Determination of limiting factors of photovoltaic efficiency in quantum dot sensitized solar cells: Correlation between cell performance and structural properties, J. Appl. Phys. 108 (2010) 064310. doi:10.1063/1.3477194.

[51] J. Bisquert, Theory of the Impedance of Electron Diffusion and Recombination in a Thin Layer, J. Phys. Chem. B. 106 (2002) 325–333. doi:10.1021/jp011941g.

[52] Q. Wang, S. Ito, M. Grätzel, F. Fabregat-Santiago, I. Mora-Sero, J. Bisquert, et al., Characteristics of High Efficiency Dye-Sensitized Solar Cells, J. Phys. Chem. B. 110 (2006) 25210–25221. doi:10.1021/jp064256o.

[53] V. González-Pedro, X. Xu, I. Mora-Sero, J. Bisquert, Modeling High-Efficiency Quantum Dot Sensitized Solar Cells, ACS Nano. 4 (2010) 5783–5790. doi:10.1021/nn101534y.

[54] F. Fabregat-Santiago, G. Garcia-Belmonte, I. Mora-Sero, J. Bisquert, Characterization of nanostructured hybrid and organic solar cells by impedance spectroscopy, Phys. Chem. Chem. Phys. 13 (2011) 9083. doi:10.1039/c0cp02249g.

**Table 1:** Characteristic Short circuit current, open circuit voltage, Fill Factor and photoconversion efficiencies of Au decorated $TiO_2$/CdS films under one sun illumination.

| **Sample** | **$J_{sc}$ mA/cm$^2$** | **$V_{oc}$ mV** | **FF %** | **η %** |
|---|---|---|---|---|
| **$TiO_2$/CdS(7)/ZnS** | 9.85 | -575 | 46.52 | 2.63 |
| **$TiO_2$/Au(0.5)/CdS(7) /ZnS** | 9.48 | -612 | 51.04 | 2.96 |
| **$TiO_2$/Au(2.5)/CdS(7) /ZnS** | 9.53 | -618 | 50.06 | 2.95 |
| **$TiO_2$/Au(7.5)/CdS(7) /ZnS** | 9.44 | -570 | 50.37 | 2.71 |

**Figure 1:** TEM image of Au nanostructured particle used to decorate the $TiO_2$ films.

**Figure 2:** Representative SEM micrographs of the transparent layer of a) $TiO_2$ films, b) $TiO_2$ decorated with Au NPs, c) CdS sensitized $TiO_2$ by SILAR, d) $TiO_2$ decorated with Au NPs and sensitized with CdS QDs and e) EDS spectrum of the $TiO_2$/Au/CdS films showing the principal peaks of Au, Cd and S.

**Figure 3:** Representative absorption spectra of $TiO_2$ films decorated with Au NPs and sensitized with CdS QDs. Showing the spectra of colloidal Au NPs.

**Figure 4:** Representative J-V curves of $TiO_2$/Au /CdS solar cells at several Au deposition times. Inset showing champion cells of $TiO_2$/Au /CdS and $TiO_2$/CdS/Au configuration.

**Figure 5:** Representative IPCE curves of CdS QDs sensitized solar cells decorated by electrophoretic deposition with Au NPs

**Figure 6:** Schematic representation of the equivalent circuit used to fit the impedance measurements, showing the principal components of the film region where the correspondent physical process occurs: the series resistance, $R_s$; the transport resistance, $R_t$;

the recombination resistance, $R_{rec}$; the chemical capacitance $C_{\mu}$; The charge transfer an capacitance at the counter electrode $R_{con}$ and $C_{con}$.

**Figure 7:** Impedance spectroscopy characterization of the $TiO_2$/Au/CdS(S)/ZnS(S) cells at 0.5, 2.5 and 7.5 min of Au NPs deposit, showing: **a)** Chemical capacitance, Cμ in the $V_f$ representation and $V_{ecb}$ representation in the inset. **b)** Recombination resistance, $R_{rec}$, also in both representations. **c)** Transport resistance $R_t$ as function of Final votage $V_f$ and inset $R_t$ as a function of voltage equivalent conduction band $V_{ecb}$.

**Figure 8:** Schematic representation of the energy levels distribution for: a) $TiO_2$/CdS cells and b) $TiO_2$/Au/CdS cells, showing the electron and hole flux (blue and red circles respectively), the energy difference between the $TiO_2$'s CB and the CdS QD's CB, $\Delta\chi$, the $TiO_2$'s quasi-Fermi level $E_F$ and the open circuit voltage $V_{oc}$.

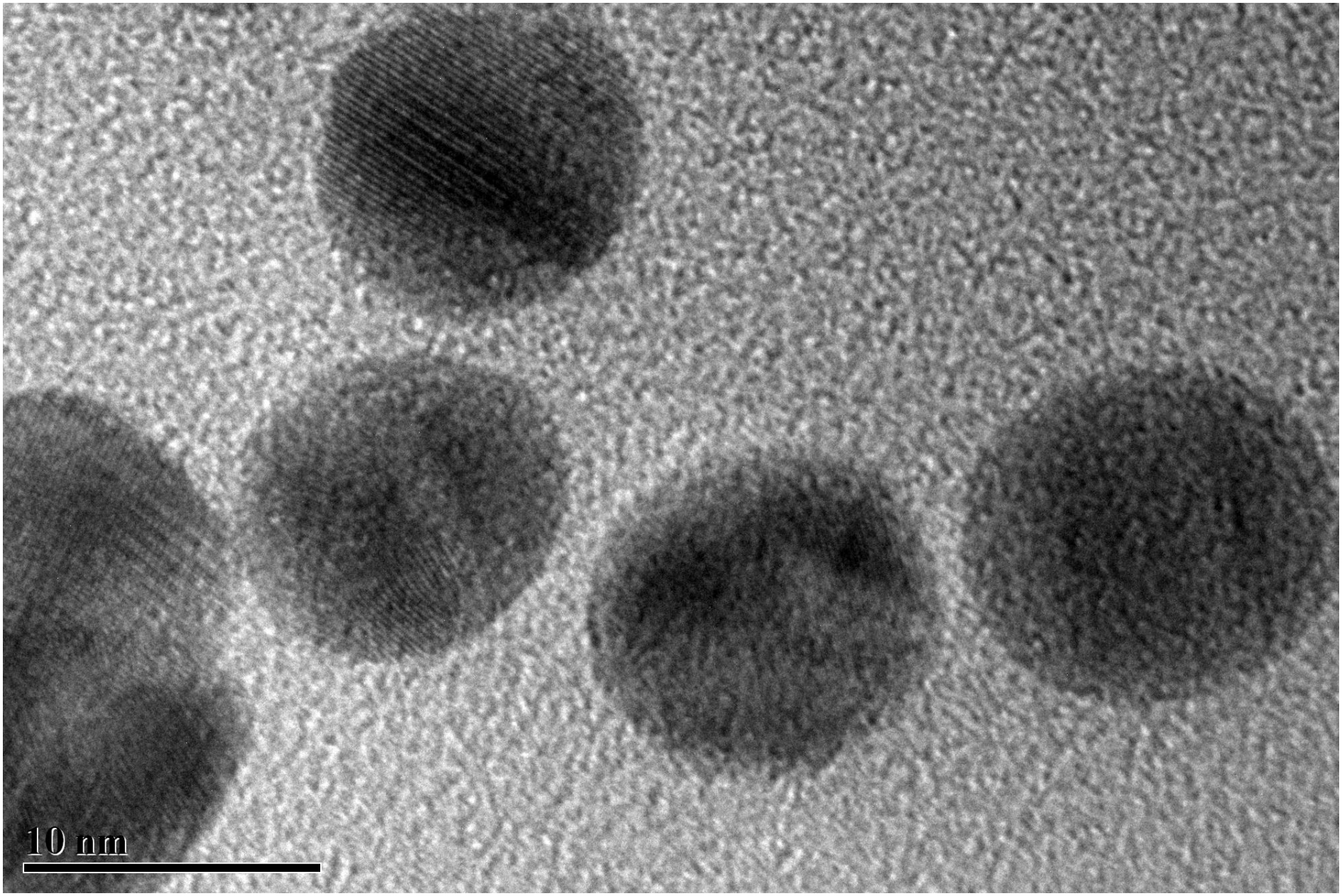
10 nm

Figure 2

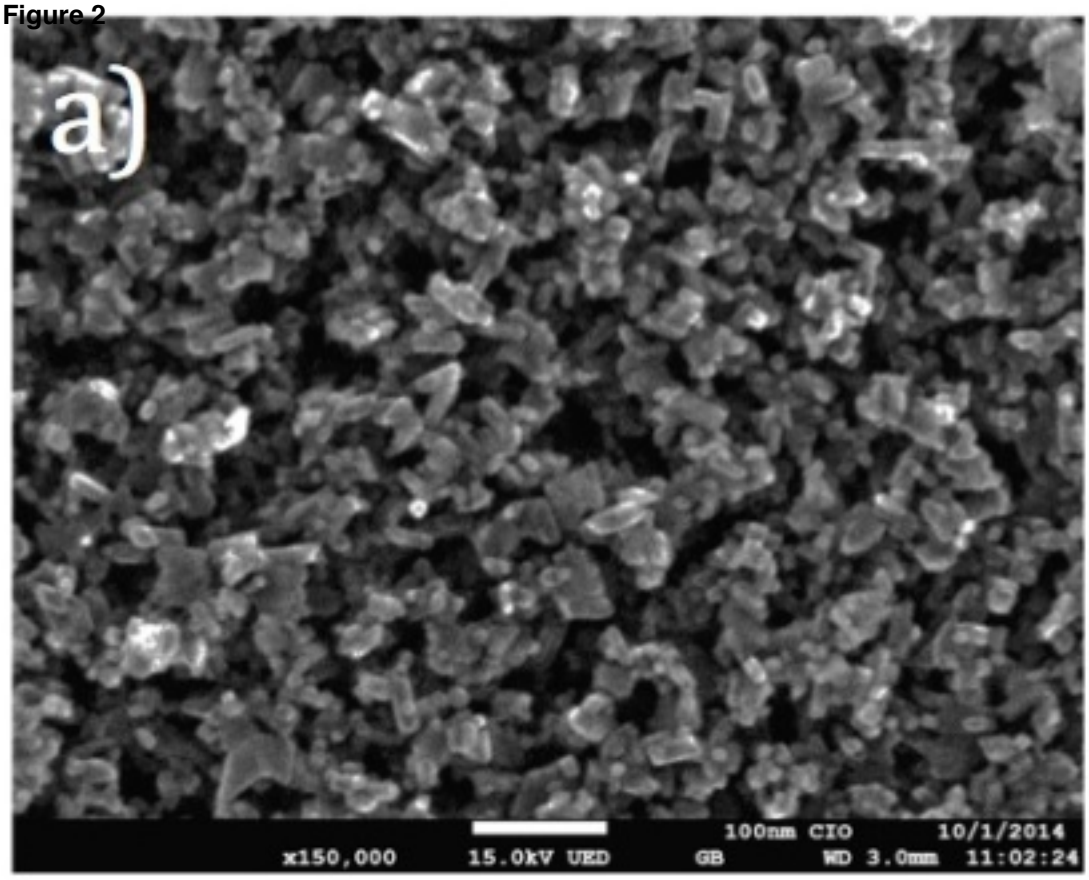
a)
100nm CIO 10/1/2014
x150,000 15.0kV UED GB WD 3.0mm 11:02:24

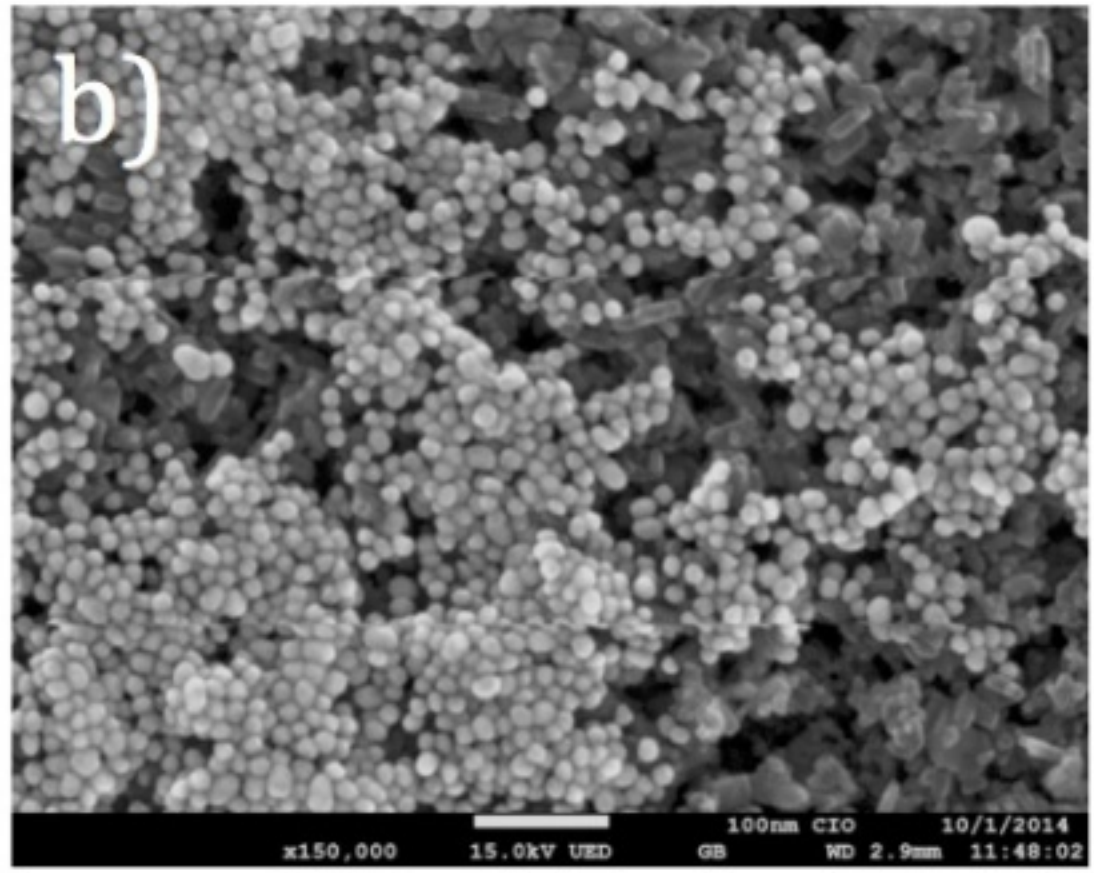
b)
100nm CIO 10/1/2014
x150,000 15.0kV UED GB WD 2.9mm 11:48:02

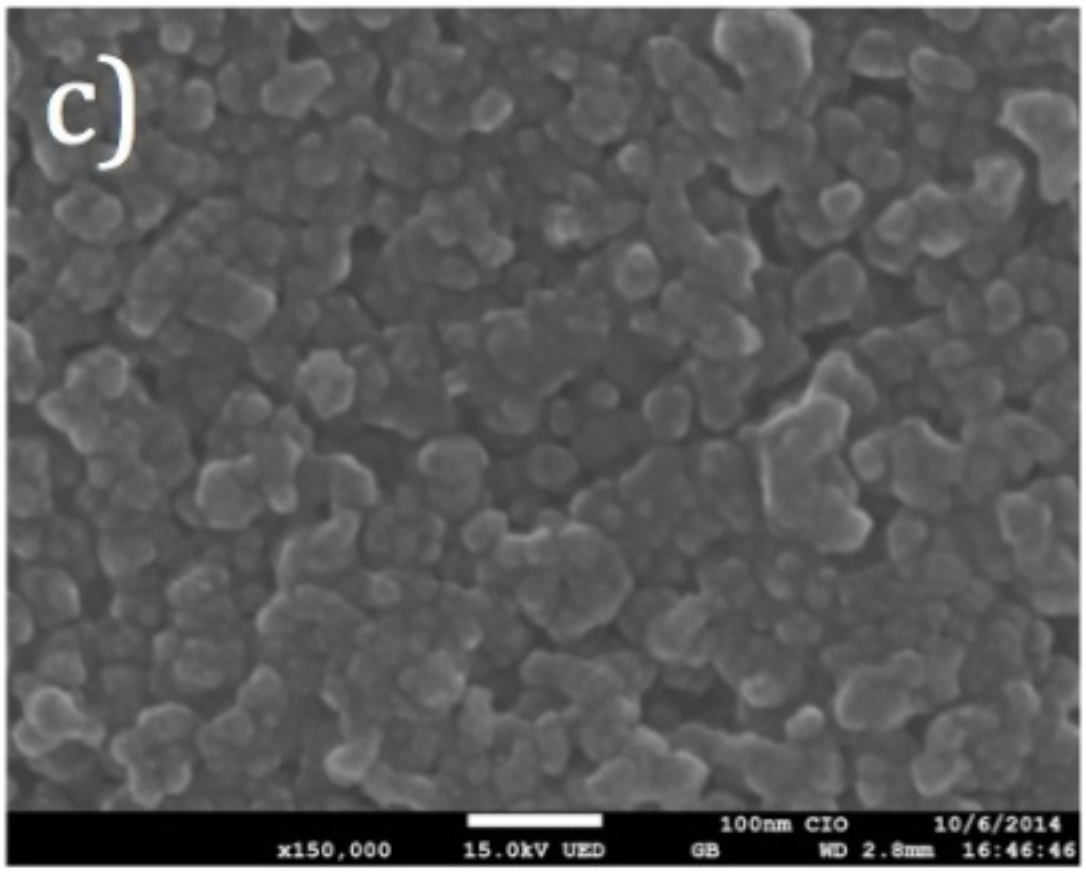
c)
100nm CIO 10/6/2014
x150,000 15.0kV UED GB WD 2.8mm 16:46:46

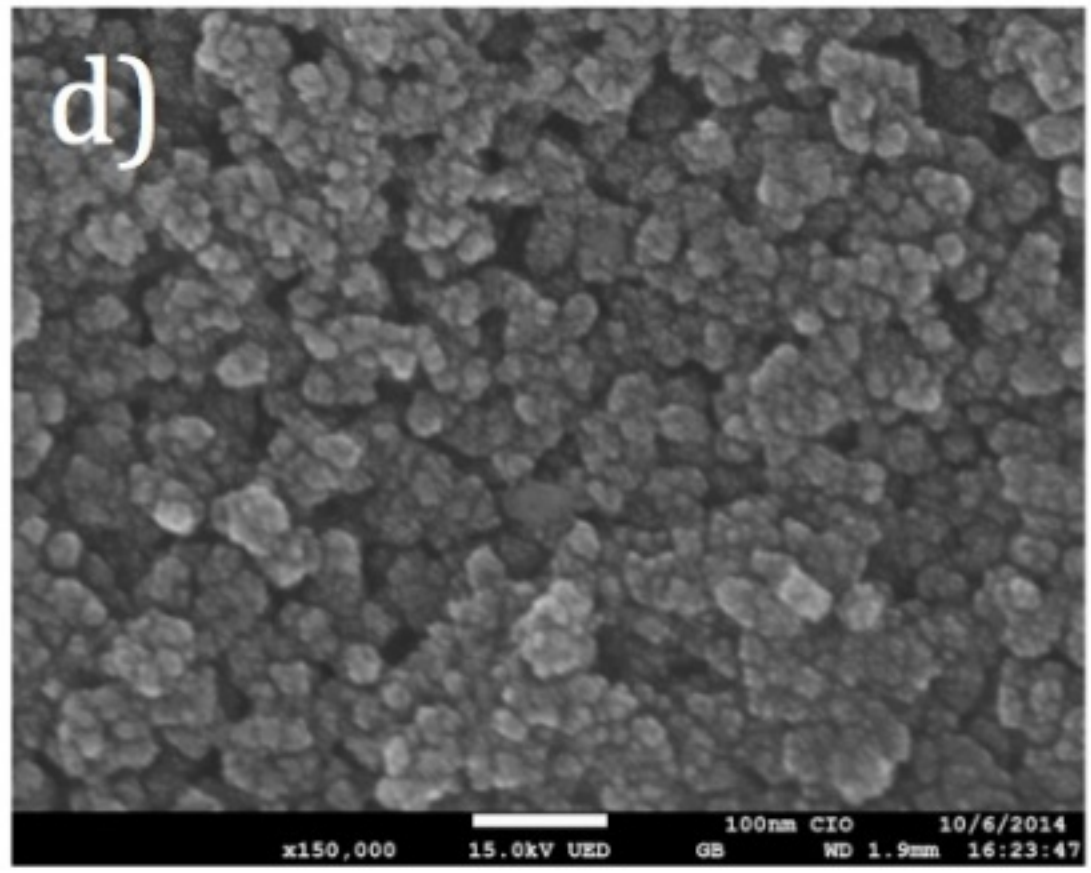
d)
100nm CIO 10/6/2014
x150,000 15.0kV UED GB WD 1.9mm 16:23:47

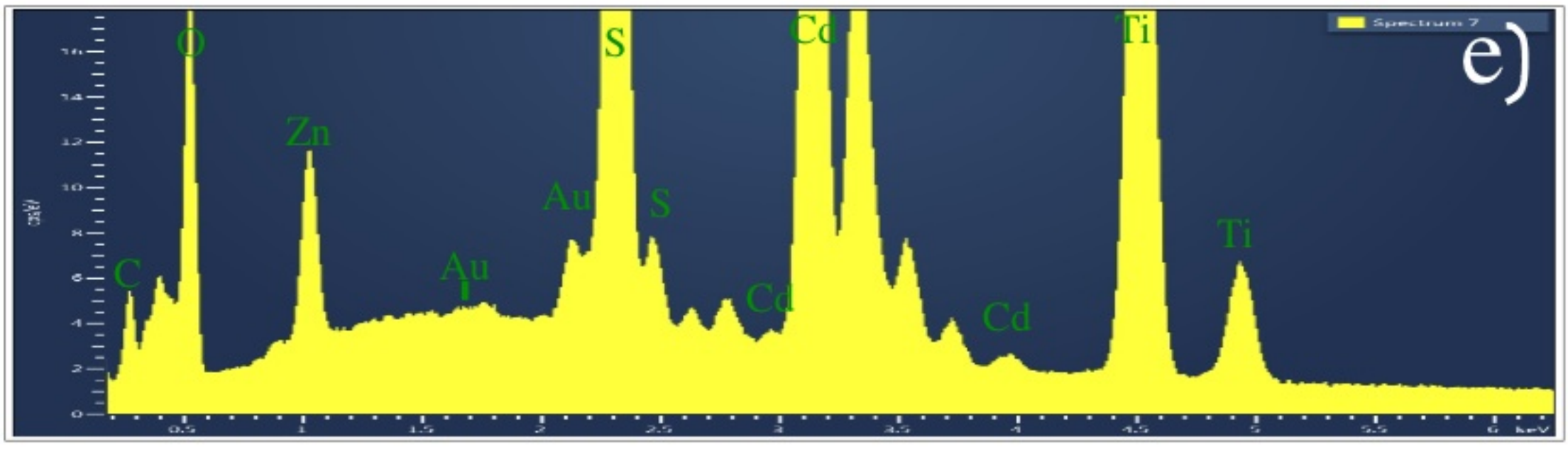
e)
Spectrum 7
O
Zn
C
Au
Au
S
S
Cd
Cd
Cd
Ti
Ti
cps/eV
keV

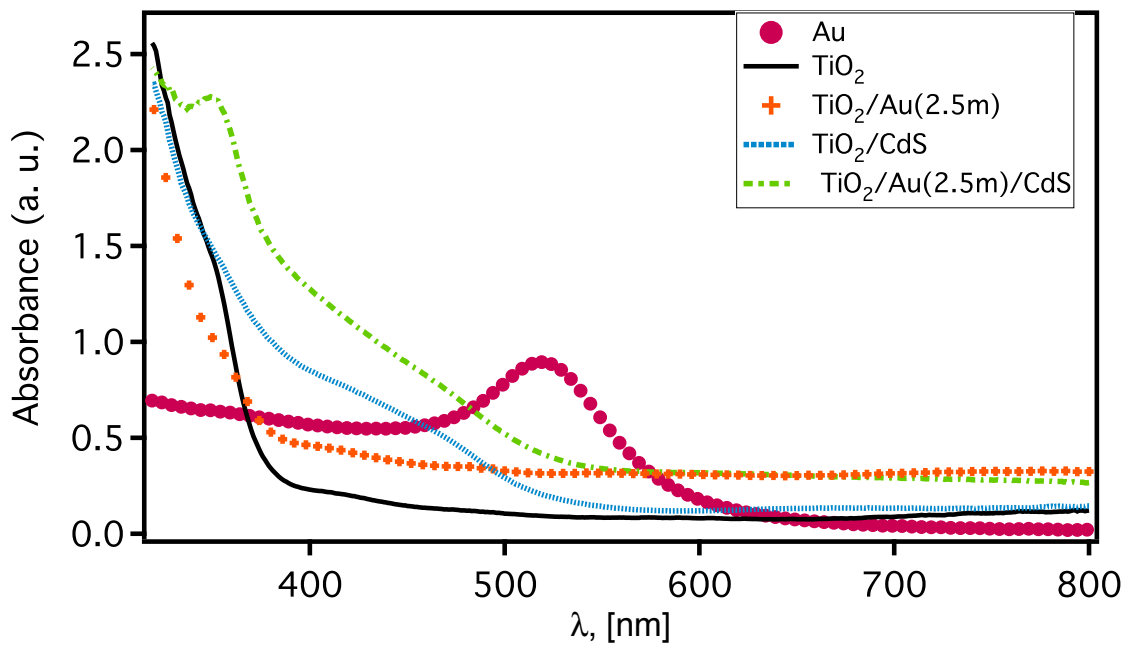
Au
TiO2
TiO2/Au(2.5m)
TiO2/CdS
TiO2/Au(2.5m)/CdS
Absorbance (a. u.)
2.5
2.0
1.5
1.0
0.5
0.0
400
500
600
700
800
λ, [nm]

Figure 4

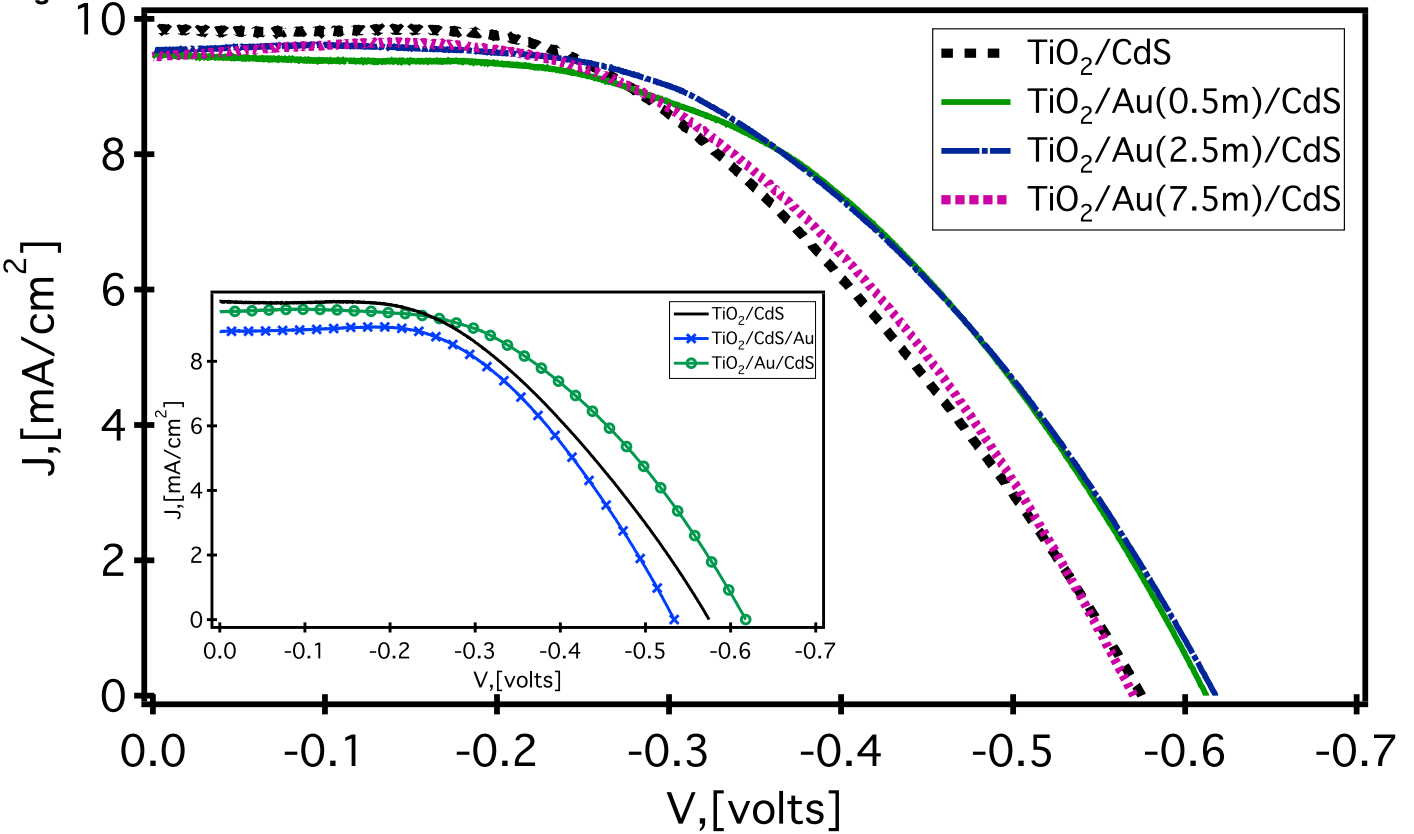
TiO2/CdS
TiO2/Au(0.5m)/CdS
TiO2/Au(2.5m)/CdS
TiO2/Au(7.5m)/CdS
J,[mA/cm2]
V,[volts]
TiO2/CdS
TiO2/CdS/Au
TiO2/Au/CdS
J,[mA/cm2]
V,[volts]

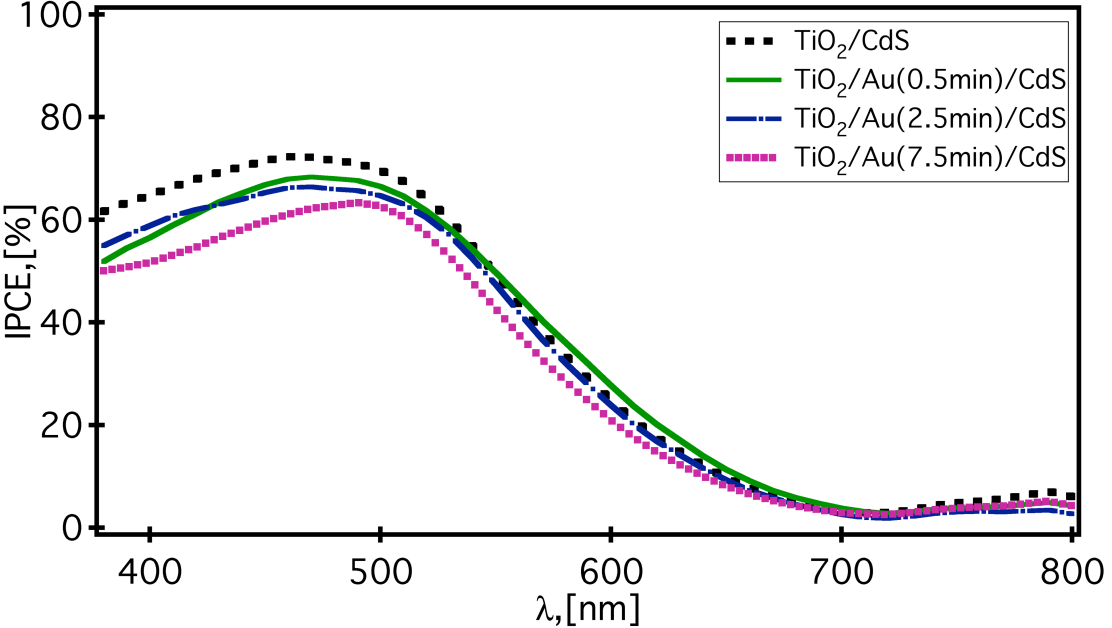
100
80
60
40
20
0
IPCE,[%]
400
500
600
700
800
λ,[nm]
TiO2/CdS
TiO2/Au(0.5min)/CdS
TiO2/Au(2.5min)/CdS
TiO2/Au(7.5min)/CdS

Figure 6

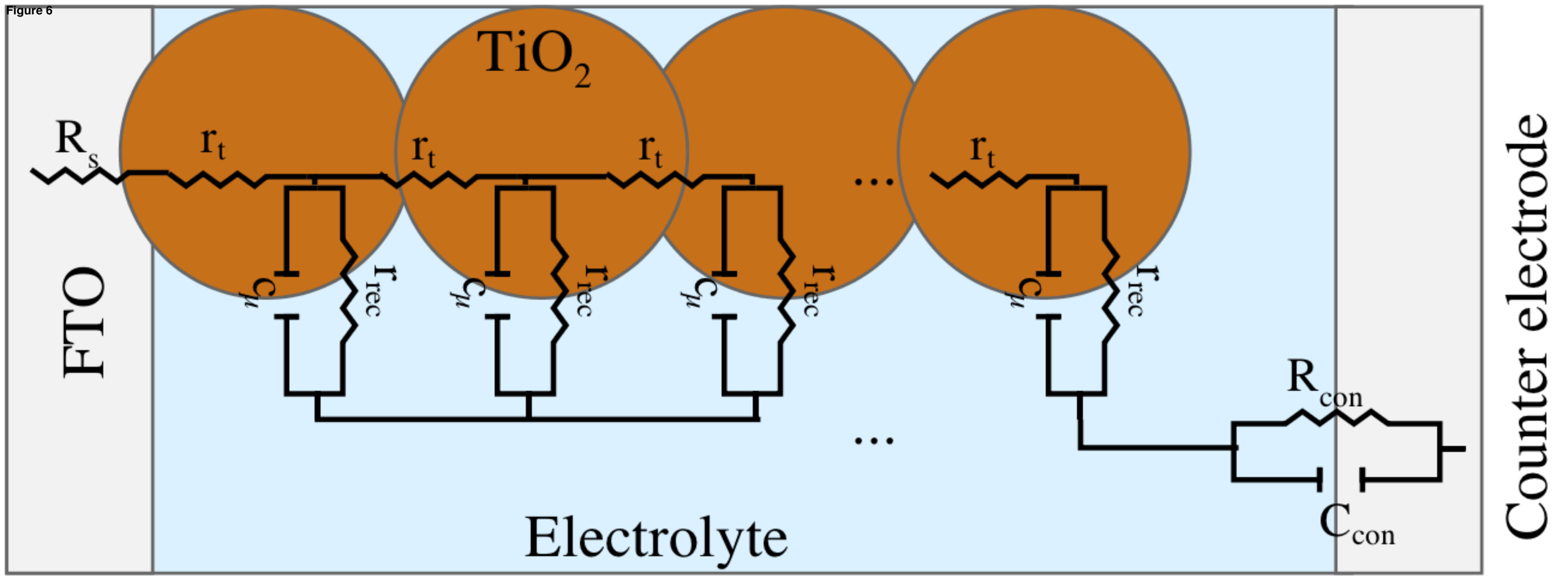
TiO2
Rs
rt
rt
rt
...
rt
FTO
Cμ
rrec
Cμ
rrec
Cμ
rrec
Cμ
rrec
...
Rcon
Ccon
Electrolyte
Counter electrode

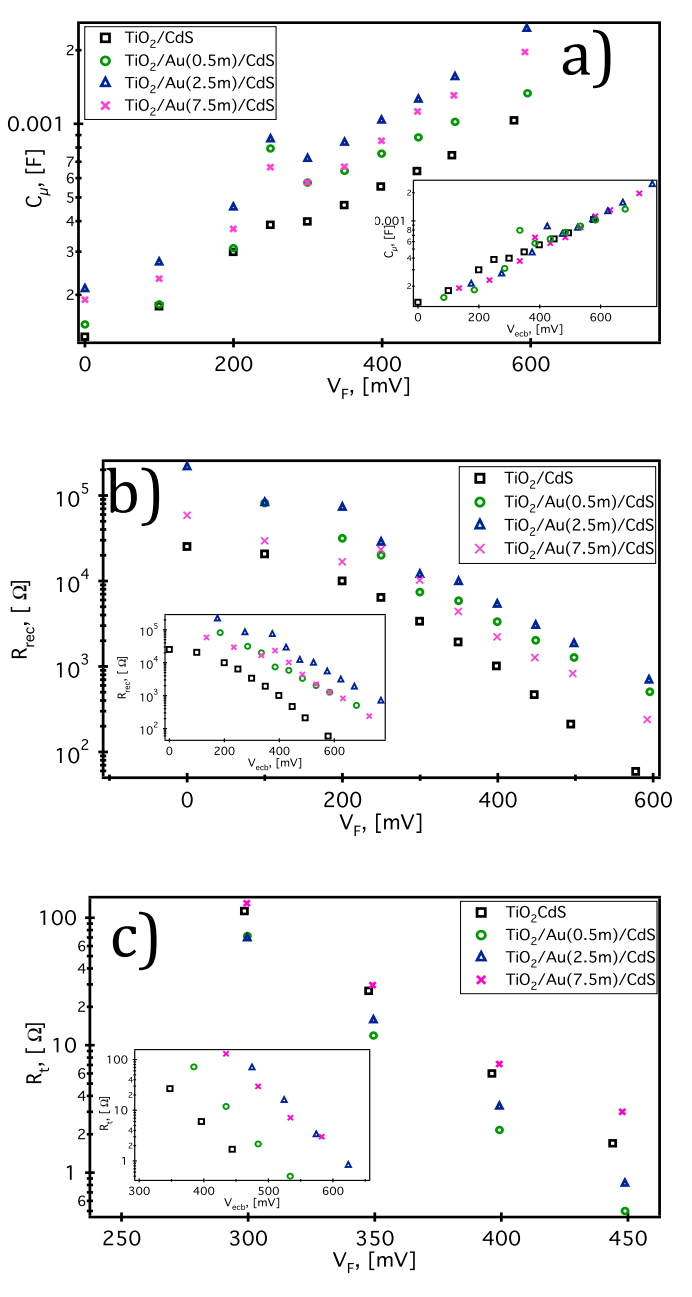
a)
TiO2/CdS
TiO2/Au(0.5m)/CdS
TiO2/Au(2.5m)/CdS
TiO2/Au(7.5m)/CdS
0.001
Cμ, [F]
0
200
400
600
VF, [mV]
Vecb, [mV]
b)
Rrec, [ Ω]
10^5
10^4
10^3
10^2
c)
Rt, [ Ω]
100
10
1
250
300
350
400
450

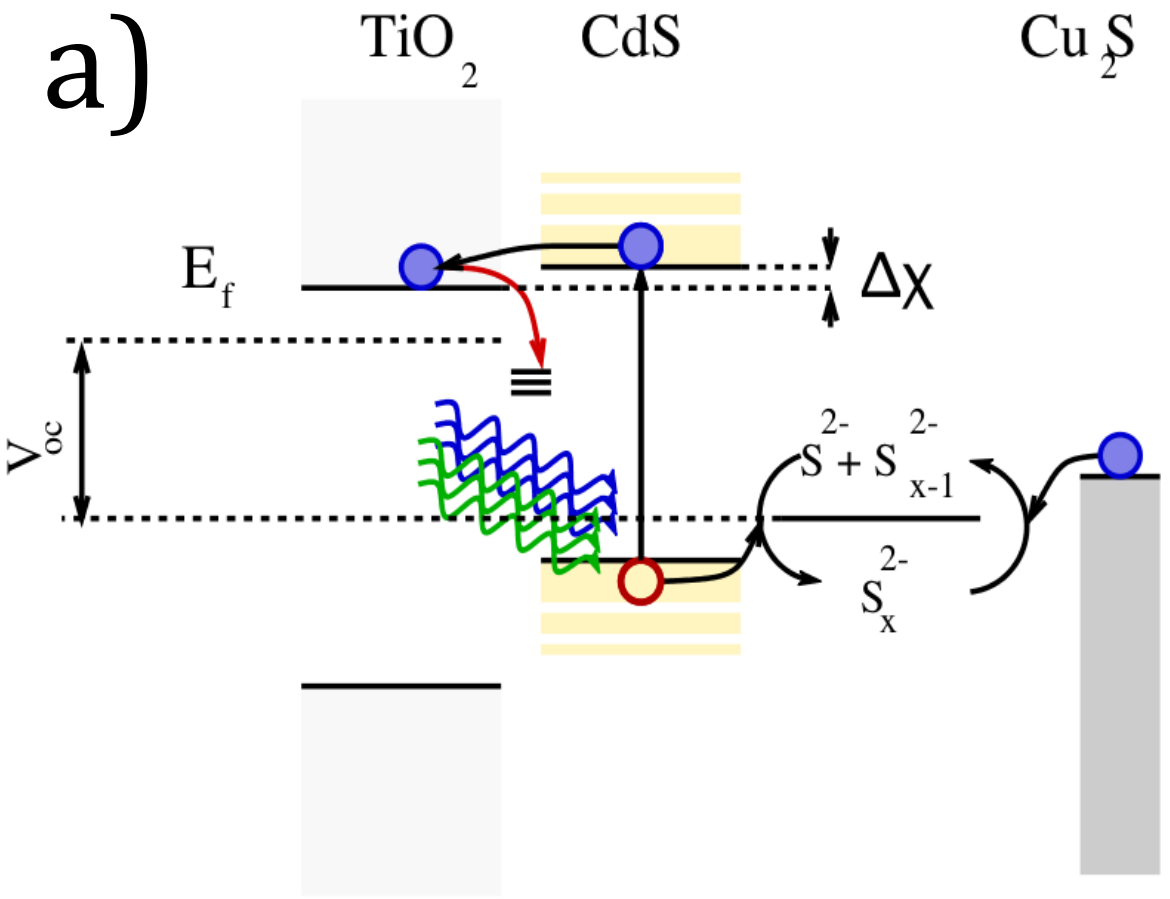
a)
TiO2
CdS
Cu2S
Ef
ΔX
Voc
S2- + Sx-12-
Sx2-

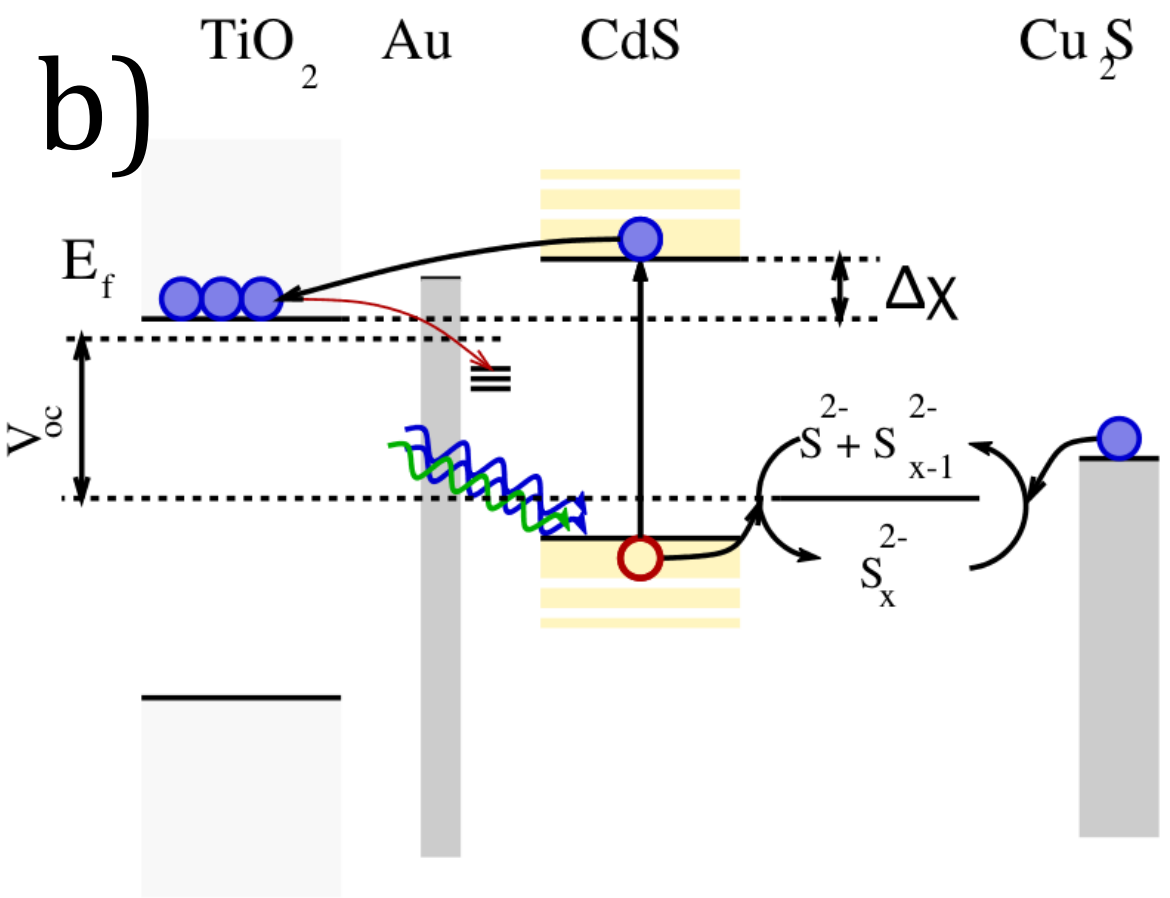
b)
TiO2
Au
CdS
Cu2S
Ef
ΔX
Voc
S2- + Sx-12-
Sx2-